Electronic Journal of Biotechnology 55 (2022) 1–8

Contents lists available at ScienceDirect

Electronic Journal of Biotechnology

journal homepage:

Research Article

Improving the low-temperature properties of an exo-inulinase *via* the deletion of a loop fragment located in its catalytic pocket

Limei He [a], Rui Zhang [a,b,c,d], Jidong Shen [a], Ying Miao [a], Chunyan Zeng [a], Xianghua Tang [a,b,c,d], Qian Wu [a,b,c,d], Junpei Zhou [a,b,c,d,*], Zunxi Huang [a,b,c,d,*]

[a] College of Life Sciences, Yunnan Normal University, Kunming 650500, People's Republic of China
[b] Engineering Research Center of Sustainable Development and Utilization of Biomass Energy, Ministry of Education, Yunnan Normal University, Kunming 650500, People's Republic of China
[c] Key Laboratory of Yunnan for Biomass Energy and Biotechnology of Environment, Yunnan, Kunming 650500, People's Republic of China
[d] Key Laboratory of Yunnan Provincial Education, Department for Plateau Characteristic Food Enzymes, Yunnan Normal University, Kunming 650500, People's Republic of China

GRAPHICAL ABSTRACT

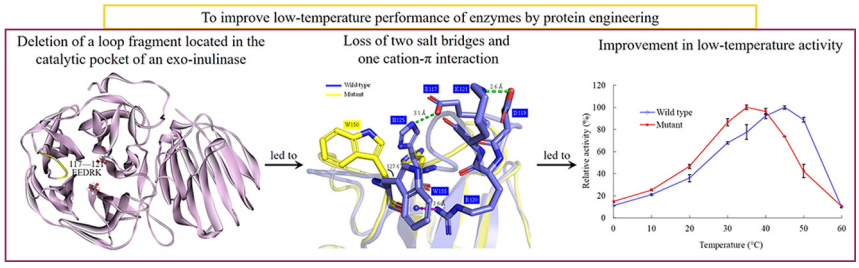

ARTICLE INFO

Article history:
Received 5 February 2021
Revised 25 March 2021
Accepted 29 September 2021
Available online 6 October 2021

Keywords:
Catalytic pocket
Deletion
Enzyme
Exo-inulinase
Glycoside hydrolase
Intraprotein interactions
Inulase
Inulin

ABSTRACT

Background: Engineering thermal adaptations of enzymes is a popular field of study. Enzymes active at low temperature have been used in many industries; however, reports seldom describe improvements in enzyme activity at low temperatures using protein engineering.
Results: Multiple amino acid sequence alignment of glycoside hydrolase (GH) family 32 showed an unconserved region located in the catalytic pocket. The exo-inulinase InuAGN25 showed the highest frequency of charged amino acid residues (47.4%) in this region among these GH 32 members. Notably, five consecutive charged amino acid residues (^{137}EEDRK^{141}) were modeled as a loop fragment in this region of InuAGN25. Deletion of the loop fragment broke two salt bridges, one cation–π interaction, and the α-helix–loop–310-helix structure at the N-terminal tail. The mutant exo-inulinase RfsMutE137Δ5 without the loop fragment was expressed in *Escherichia coli*, digested using human rhinovirus 3C protease for removal of the fused sequence at the N-terminus, and purified using immobilized metal affinity chromatography. Compared to the wild-type enzyme, the optimum temperature and $t_{1/2}$ at 50°C of purified RfsMutE137Δ5 decreased by 10°C and 31.7 min, respectively, and the activities at 20°C and 30°C increased by 11% and 18%, respectively.

Peer review under responsibility of Pontificia Universidad Católica de Valparaíso
* Corresponding authors.
E-mail addresses: junpeizhou@ynnu.edu.cn (J. Zhou), huangzunxi@163.com (Z. Huang).

https://doi.org/10.1016/j.ejbt.2021.09.004

Loop fragment
Low-temperature
Mutagenesis
Protein engineering
Thermostability

Conclusions: In this study, we engineered the loop to obtain the mutant exo-inulinase that showed an improved performance at low temperatures. These findings suggest that the loop may be a useful target in formulating rational designs for engineering thermal adaptations of GH 32 exo-inulinases.

How to cite: He L, Zhang R, Shen J. et al. Improving the low-temperature properties of an exo-inulinase via the deletion of a loop fragment located in its catalytic pocket. Electron J Biotechnol 2022;55. https://doi.org/10.1016/j.ejbt.2021.09.004

1. Introduction

As the second most abundant storage polysaccharide in nature, inulin is present in tubers, bulbs, and tuberous roots of more than 36,000 plants, such as Jerusalem artichoke, chicory, and dahlia [1]. Jerusalem artichoke (*Helianthus tuberosus*) is a nongrain crop with rapid growth, strong environmental tolerance, and high resistance to pests and diseases [2]. Furthermore, the crop can be harvested three times a year with the production of inulin-rich biomass [2]. Approximately 80% of the total carbohydrates in the tuberous roots of Jerusalem artichoke is inulin, which can be dissolved in hot water; therefore, the extraction of inulin is easy and inexpensive [2]. The utilization of inulin has attracted great attention in recent years [1,2].

Structurally, inulin consists of polymerized fructose moieties with β-D-(2 → 1) linkages and a terminal glucose moiety at the reducing end with α-D-(2 → 1) linkage [1,2]. The degradation of inulin yields fructose, which plays an important role in the food, chemical, and pharmaceutical industries, such as precursor for the production of acetone, ethanol, single cell oils, sorbitol, lactic acid, and succinic acid *via* microbial utilization [1,2].

Terminal 2,1-linked β-D-fructose residues in inulin can be hydrolyzed one by one using glycoside hydrolase (GH) family 32 exo-inulinases, yielding fructose at concentrations as high as 90–95% [1]. Compared to conventional acid hydrolysis, exo-inulinase hydrolysis of inulin is advantageous in some aspects, such as for deriving higher fructose yield, making the process for fructose separation easier, suiting biorefinery better, and lowering refining costs [1].

Enzymes showing high activity in low temperature environments, which form > 80% of the Earth's biosphere [3], have been used for cleaning, energy saving, preventing degradation of food and modifications to flavor during food processing, and producing stereospecific chiral compounds for fine-chemical organic synthesis [4]. Therefore, it is important to improve activity of enzymes at low temperatures, usually by increasing their structural flexibility [3]. To date, most reports describe improvement in thermostability and substrate recognition mechanisms upon engineering exo-inulinases [5,6,7], while few reports describe improvement in performance at low temperatures [8,9].

In our previous study, we characterized a novel exo-inulinase (InuAGN25) and showed its ability to hydrolyze inulin at 0°C and 10°C with the production of fructose [10]. The following study on sequential deletion of N-terminal amino acid residues showed that the number of salt bridges and cation–π interactions within the N-terminal tail increased with improved thermostability [11]. Another study designed a mutant with the change in eight amino acid residues and showed that the flexibility of the catalytic domain increased with improved activity at low temperatures on the basis of molecular dynamics simulation data [8]. In this study, the aim was to reveal the key loop involved in the formation of salt bridges and cation–π interactions in the catalytic pocket and to improve the performance of the exo-inulinase at low temperatures.

2. Materials and methods

2.1. Chemicals

Inulin from dahlia tubers, human rhinovirus 3C protease (HRV 3C protease), isopropyl-β-D-1-thiogalactopyranoside (IPTG), nickel-NTA agarose, and silica gel G plates were supplied by Sigma-Aldrich (St. Louis, MO, USA), TaKaRa (Otsu, Japan), Amresco (Solon, OH, USA), Qiagen (Valencia, CA, USA), and Haiyang (Qingdao, China), respectively, and other chemicals (analytical grade) were purchased from commercial suppliers.

2.2. Bacterial strains and vectors

*p*ET-28a(+), supplied by Synbio Technologies (Suzhou, China), was used as a heterologous expression vector.

Escherichia coli BL21 (DE3) (Synbio Technologies) was grown in Luria–Bertani medium supplemented with 100 μg mL^{-1} kanamycin (LBK medium) for heterologous expression. The strain *Sphingobacterium* sp. GN25 harboring InuAGN25 (GenBank accession no. AGC01503) was grown in an inulin-inducing medium [10]. This strain has been deposited in the China General Microbiological Culture Collection Center under CGMCC 1.10975 [10].

2.3. Prediction of the loop for mutagenesis

Multiple amino acid sequences from GH 32 were aligned using Clustal X [12] to show the differences between InuAGN25 and other GH 32 members. Seed sequences of GH 32 used for alignment were downloaded from the Pfam database (http://pfam.xfam.org/family/PF00251). The tertiary structure of the mutant enzyme was predicted using the I-TASSER platform (http://zhanglab.ccmb.med.umich.edu/I-TASSER/), and intraprotein interactions including salt bridges (distance cut-off: 3.2 Å) and energetically significant cation–π interactions (distance cut-off: 6.0 Å) were predicted using VMD [13] and CaPTURE [14], respectively. To validate the predictions, intraprotein interactions were identified using Protein Interactions Calculator [15]. pK_a values of amino acid residues at pH 7.0 were calculated using PROPKA [16].

2.4. Construction of the expression plasmid

The recombinant plasmid for heterologous expression of mature InuAGN25 (MInuAGN25; removal of the predicted signal peptide) was constructed using *p*ET-28a(+) as the vector [11]. In consideration of the effects of terminal fusion sequence on thermal performance of enzymes [11,17], the HRV 3C protease recognition site (LEVLFQGP) and a stop codon were inserted into the N-terminus and C-terminus of the recombinant MInuAGN25 (HHMInuAGN25), respectively. HRV 3C protease is active at a low temperature; HRV is well known for the removal of fusion sequences at low temperatures in order to reduce thermal denaturation of samples [18,19].

Using the recombinant plasmid of HHMInuAGN25 as the template, the mutant plasmid was constructed by Synbio Technologies. Briefly, the nucleic acid sequence encoding the mutant enzyme, designated as MutE137Δ5, was synthesized with the addition of *Nco*I and *Xho*I recognition sites at the 5′ terminus and 3′ terminus, respectively. The sequence was then ligated to *p*ET-28a(+) *via* the traditional restriction-ligation step using endonucleases and T4 DNA ligase. The mutant plasmid was sequenced by Tsingke (Beijing, China) and the nucleic acid bases were verified.

2.5. Heterologous expression and mutant enzyme extraction

The plasmid expressing recombinant MutE137Δ5 (HHMutE137Δ5) was transformed into *E. coli* BL21 (DE3) after the traditional heat shock procedure. Positive clones were screened by PCR using universal primers T7 and T7ter. Production of the mutant enzyme was induced at approximately 20°C for an appropriate duration using IPTG at the final concentration of 0.7 mM when the positive *E. coli* clone grown in LBK medium reached the exponential phase of growth. After induction, the culture was centrifuged for harvesting recombinant *E. coli* cells. The *E. coli* cells were lysed using sonication on ice to extract intracellular substances including HHMutE137Δ5.

2.6. Removal of fusion sequence and purification of mutant enzyme

The mutant enzyme HHMutE137Δ5 tagged with His_6 was loaded and bound to a nickel-NTA agarose gel and then eluted with a solution of pH 7.2 containing 20 mM Tris–HCl, 0.5 M NaCl, 10% (w/v) glycerol, and 20–500 mM imidazole. Subsequently, purified HHMutE137Δ5 was incubated with HRV 3C protease at 4°C for around 16 h to cleave the fusion amino acid sequence, MGSSHHHHHHSSGLVPRGSHMASMTGGQQMGRGSEFLEVLFQ with a molecular weight of 4.6 kDa, from the N-terminus of the mutant enzyme. After one more round of immobilized metal affinity chromatography, the cleaved fusion sequence and the protease in the digestion solution were bound to a Ni^{2+}-NTA agarose gel, while HHMutE137Δ5 without the fusion sequence, designated as RfsMutE137Δ5, was eluted using the same elution solution mentioned above and identified using sodium dodecyl sulfate–polyacrylamide gel electrophoresis (SDS–PAGE). Regarding the effects of NaCl and glycerol on thermostability of the enzyme [10], the elution solution was replaced by McIlvaine buffer (pH 7.0) through the dialysis method.

2.7. Mode of action of purified RfsMutE137Δ5

To date, both exo- and endo-inulinases are grouped into the GH 32 family; however, the mechanisms for the exo- and endo-action modes and related key residues have not been reported. Therefore, to determine whether the mutagenesis changed the mode of action, 0.5% inulin (w/v) was incubated with purified RfsMutE137Δ5 at 37°C in pH 6.0 McIlvaine buffer for 4 h. The products of hydrolysis were then detected using thin layer chromatography (TLC). TLC was performed at room temperature as described previously, by using the silica gel G plate, n-butanol/acetic acid/water (2:1:1), and aniline–diphenylamine–phosphoric acid–acetone solution as the TLC plate, developing reagent, and chromogenic agent, respectively [10].

2.8. Characterization of purified RfsMutE137Δ5

Characteristics of purified RfsMutE137Δ5 were determined in triplicates by spectrophotometry at 540 nm performed using half the volume of the reaction system as described previously. One unit of exo-inulinase activity was defined as the amount of enzyme that released 1 μmol of fructose per minute [10]. Briefly, 450 μl 0.5% (w/v) inulin solution was mixed with 50 μl of purified RfsMutE137Δ5; after 10 min, 750 μl of 3,5-dinitrosalicylic acid (DNS) reagent was added to stop the reaction. The mixture was boiled for 5 min, and the mixture was then cooled down to room temperature for the measurement of absorption at 540 nm.

The conditions for determining pH- and temperature-dependent activity and stability of purified RfsMutE137Δ5 were the same as those for the wild-type RfsMInuAGN25 (removal of amino acid fusion sequence from HHMInuAGN25 by HRV 3C protease) as described previously [11]. The pH-dependent activity of purified RfsMutE137Δ5 for inulin was determined in triplicates at 37°C using the McIlvaine buffer (pH 5.0–8.0). pH stability of purified RfsMutE137Δ5 was assessed in triplicates by measuring residual activity at 37°C and pH 6.0 after incubation of the enzyme in McIlvaine buffer (pH 3.0–8.0), and 0.1 M glycine–NaOH buffer (pH 9.0–11.0), at 20°C for 1 h without substrate. The temperature-dependent activity of purified RfsMutE137Δ5 for inulin was determined in triplicates in pH 6.0 McIlvaine buffer at 0°C to 60°C. Thermostability of enzyme was determined in triplicates by measuring residual activity at 37°C and McIlvaine buffer (pH 6.0) after incubation of the enzyme at 45°C or 50°C for 10–60 min without substrate. Half-life ($t_{1/2}$) of enzyme at 50°C was calculated according to the thermostability data using the equation described previously [9]: $t_{1/2} = \ln 0.5/(-k_d)$, where k_d is the slope plotted with lnA/A0 versus time, and A/A0 is the relative residual activity (%) at each time point.

3. Results

3.1. Multiple amino acid sequence alignment

Multiple amino acid sequence alignment of GH 32 showed an interesting nonconserved region; the frequencies of each amino acid in most of the alignment positions in this region were not higher than 50% (Fig. 1). Only 13 of these GH 32 members (81 sequences) had a high frequency (>36%) of charged amino acid residues (D, E, H, K, and R) in this region, with highest frequency (47.4%) observed for InuAGN25. Notably, five consecutive charged amino acid residues, ^{137}EEDRK^{141} of InuAGN25, attracted our attention because this was hardly observed in other GH 32 members (Fig. 1).

3.2. Structural analysis

The homology model of the wild-type RfsMInuAGN25 was built successfully with a high confidence using the I-TASSER platform [11]. This model comprised two distinct domains: the N-terminal 5-fold β-propeller and the C-terminal β-sandwich structure (Fig. 2). The catalytic residues D31 and E210 were predicted and located in the catalytic pocket of the N-terminal 5-fold β-propeller (Fig. 2). The five consecutive charged amino acid residues, ^{137}EEDRK^{141} of InuAGN25 (corresponding to ^{117}EEDRK^{121} of RfsMInuAGN25), were modeled as a Ω-loop fragment located in the catalytic pocket (Fig. 2).

By using the I-TASSER platform, the homology model of the mutant enzyme RfsMutE137Δ5 without the ^{117}EEDRK^{121} fragment was also built successfully with a high confidence. The C-score and estimated TM-score for the model were 1.14 and 0.87, respectively. Removal of the ^{117}EEDRK^{121} fragment led to the shortened loop in the model of RfsMutE137Δ5 (Fig. 2). Notably, the α-helix–loop–3 10-helix structure within the N-terminal tail of RfsMInuAGN25 was not constructed for RfsMutE137Δ5 (Fig. 2).

There were 43 and 40 salt bridges detected in the tertiary structures of RfsMInuAGN25 and RfsMutE137Δ5, respectively. RfsMI-

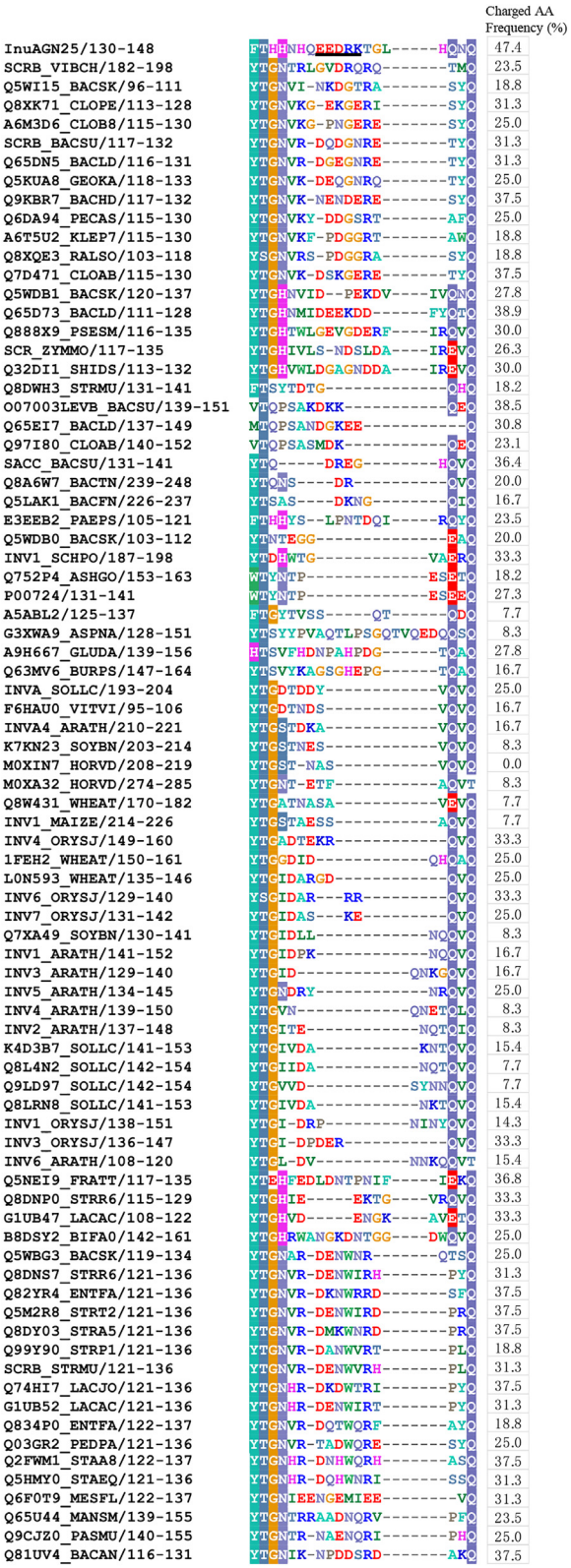

Fig. 1. Partial alignment of amino acid residues including ^{137}EEDRK^{141} of InuAGN25 with GH 32 members. Seed sequences of GH 32 used for the alignment were downloaded from the Pfam database (http://pfam.xfam.org/family/PF00251). Charged AA Frequency is the total frequency of amino acid residues D, E, R, K, and H in the alignment region of each sequence.

nuAGN25 had three more salt bridges than RfsMutE137Δ5. As shown in Fig. 3, two of these three salt bridges were related to ^{117}EEDRK^{121}: one salt bridge was formed by residues D119 and K121, and the other one was formed by residues E117 and H125 (the pK_a value of H125 at pH 7.0 was predicted as 7.19). Furthermore, the residue R120 in ^{117}EEDRK^{121} interacted with W155 through a cation–π interaction in RfsMInuAGN25. However, the cation–π interaction was not observed in RfsMutE137Δ5 without R120. Thus, W150 from RfsMutE137Δ5 was not restrained by the cation–π interaction with R120, and it rotated by 127.6° as compared to W155 from RfsMInuAGN25 (Fig. 3).

3.3. Heterelogous expression and purification of RfsMutE137Δ5

The plasmid expressing HHMutE137Δ5 was successfully constructed using *p*ET-28a(+) as a vector, with the HRV 3C protease recognition site inserted into the N-terminus of the recombinant enzyme. By using *E. coli* BL21 (DE3) as a host, HHMutE137Δ5 was expressed in cells with a His_6 tag and purified successfully using immobilized metal affinity chromatography (Fig. 4). After the HRV 3C protease digestion, the amino acid fusion sequence (approximately 4.6 kDa) was removed from HHMutE137Δ5 (Fig. 4). RfsMutE137Δ5 was then purified through one more round of immobilized metal affinity chromatography to obtain the electrophoretically pure protein (Fig. 4).

3.4. Mode of action of purified RfsMutE137Δ5

Deletion of ^{117}EEDRK^{121} did not change the exo-action mode of RfsMutE137Δ5, and it degraded inulin to yield fructose (Fig. 5).

3.5. Enzymatic properties of RfsMutE137Δ5

pH-dependent activity and stability curves of purified RfsMutE137Δ5 were similar to those of RfsMInuAGN25. Both the enzymes were most active at pH 6.0–6.5 and stable at pH 4.0–10.0 (Fig. 6A, B).

The temperature-dependent activities of purified RfsMInuAGN25 and RfsMutE137Δ5 were markedly different: RfsMutE137Δ5 was more active at low temperatures but less active at high temperatures as compared to RfsMInuAGN25. As shown in Fig. 6C, the maximal activities of purified RfsMInuAGN25 and RfsMutE137Δ5 were observed at 45°C and 35°C, respectively. Furthermore, RfsMInuAGN25 showed 11%, 21%, 36%, 68%, 78%, and 89% activity at 0°C, 10°C, 20°C, 30°C, 35°C, and 50°C, respectively, while RfsMutE137Δ5 showed 15%, 25%, 47%, 86%, 74%, and 42% activity at 0°C, 10°C, 20°C, 30°C, 45°C, and 50°C, respectively (Fig. 6C).

A comparison of thermostability of purified RfsMInuAGN25 and RfsMutE137Δ5 is shown in Fig. 6D. Both RfsMInuAGN25 and RfsMutE137Δ5 were stable at 45°C. However, $t_{1/2}$ of RfsMInuAGN25 and RfsMutE137Δ5 at 50°C were 75.3 min and 43.6 min, respectively (Fig. 6D).

4. Discussion

Arjomand et al. [9] indicated that nine Ω-loops are present in the N-terminal 5-fold β-propeller structure of the exo-inulinase from *Aspergillus niger* 5012, and all the nine Ω-loops showed low occurrence of the charged residues. For example, the Ω-loop 5, formed by ^{114}PVAQTLPSGQTVQED^{128} of *A. niger* 5012 exo-inulinase, has only two charged residues [9]. The Ω-loop, partially formed by ^{137}EEDRK^{141} of InuAGN25, corresponds to the Ω-loop 5 of *A. niger* 5012 exo-inulinase. Furthermore, the amino acid composition analysis indicates that InuAGN25 has the highest frequency of charged amino acid residues in the region among 81 GH 32 members as shown in Fig. 1. Therefore, five consecutive

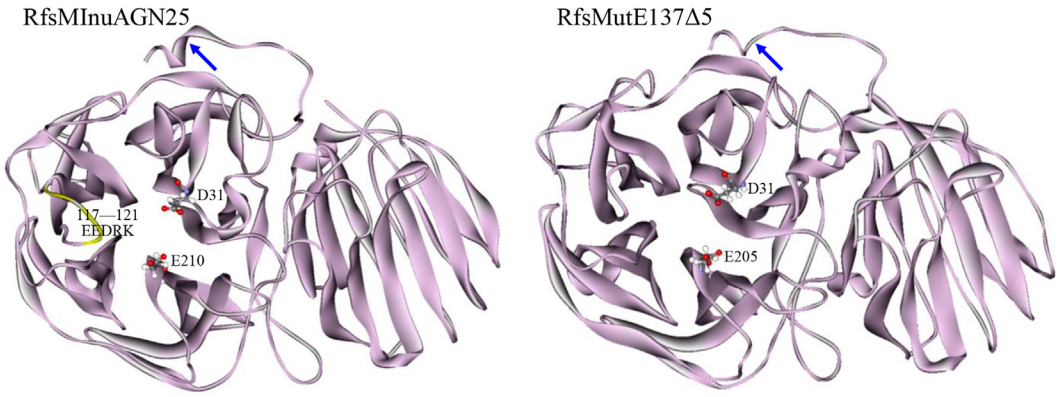

Fig. 2. Tertiary structures of the wild-type RfsMInuAGN25 and its mutant RfsMutE137Δ5. Amino acid residues ^{117}EEDRK^{121}, D31, and E210 of RfsMInuAGN25 correspond to ^{137}EEDRK^{141}, D51, and E230 of InuAGN25, respectively. The arrows indicate the changes in secondary structures.

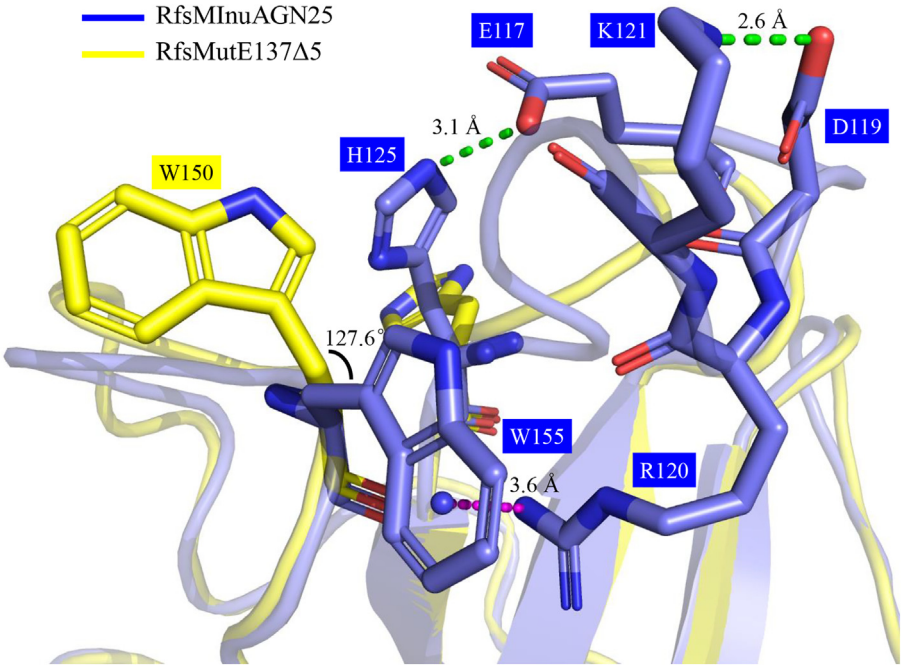

Fig. 3. Partial structural alignment of the wild-type RfsMInuAGN25 (blue) and mutant RfsMutE137Δ5 (yellow). The amino acid residues involved in salt bridges and cation-π interactions are shown in stick form. Green-dotted lines indicate the salt bridges. Purple-dotted line indicates the cation-π interaction.

charged amino acid residues are not usually noticed in the GH 32 family, and their effects should be studied.

Usually, amino acid residues in loops are hotspots for engineering thermostability in enzymes because these residues show low conservation and most of them have high flexibility that makes loops tend to unfold first during thermal denaturation [20,21,22]. Shortening loop lengths is believed to be an efficient way to improve the thermostability of enzymes [23], however, this is not always the case [24]. For example, the thermostability of phospholipase D from *Streptomyces antibioticus* PLD is improved when the loop formed by D37–G45 is deleted [25]. The thermostability of acylphosphatase from human muscle is also improved upon shortening loop 4 (residues 64–77) [26]; however, deletion of the Ω-loop 3 fragment (^{74}YGSDVT^{79}) containing an aspartic acid residue adjacent to its active site diminishes the thermostability of *A. niger* 5012 exo-inulinase [9]. In this study, removal of the Ω-loop 5 fragment ^{117}EEDRK^{121} led to loss of thermostability of RfsMutE137Δ5 at 50°C.

Deletion of the Ω-loop 3 fragment of *A. niger* 5012 exo-inulinase affects the pattern of hydrogen bonding between the active site residues and the substrate [9]. However, the effects of the Ω-loop 5 fragment ^{117}EEDRK^{121} deletion on the structure of the enzyme are different from those of Ω-loop 3. Generally, the formation of salt bridges, cation–π interactions, and helix structures contributes to enhanced thermostability of protein as they can increase global or local rigidity of protein structure [20,23,27]. For example, more salt bridges are observed in mutants H112Y and F113Y that are more active and stable at high temperatures than those seen in wild-type GH 5 β-mannanase from *Penicillium* sp. WN1 [28]; cation-π interactions are observed for mutants H58Y, T71Y, and T304Y that are more active and stable at high temperatures than the wild-type GH 28 endo-polygalacturonase from *Penicillium* sp. CGMCC 1669 [29]. The previously prepared mutant RfsMutNGln23Δ3 with the removal of 3 amino acid residues of the N-terminal tail shows enhanced thermostability mainly owing to the formation of salt bridges, cation–π interactions, and helix

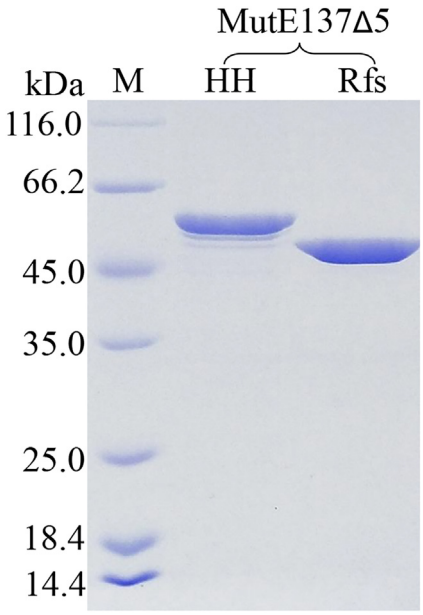

Fig. 4. SDS-PAGE analysis. M, protein molecular weight marker; HH, purified HHMutE137Δ5; Rfs, purified RfsMutE137Δ5.

structures that enhance the rigidity of the N-terminal tail [11]. Therefore, RfsMutE137Δ5 shows thermostability in contrast to those of RfsMutNGln23Δ3.

Decrease in intraprotein interactions in the catalytic pocket resulted in a 10°C decrease in optimum temperature and activity increase at low temperatures for the mutant RfsMutE137Δ5 as compared to that seen for wild-type RfsMInuAGN25. Most exo-inulinases exhibit their optimal activities in the temperature range of 40°C to 60°C [30,31]. To the best of our knowledge, only the exo-inulinase isolated from *Arthrobacter* sp. MN8 is the most active at 35°C [32]. Furthermore, typical low temperature-active enzymes should be much more active at temperatures lower than 30°C; however, they are less thermostable at temperatures higher than 40°C as compared to their mesophilic homologues [33]. Atypical low temperature-active enzymes such as RfsMInuAGN25 maintain a high activity at low temperatures as well as good thermostability at temperatures higher than 40°C. Compared to enzymes that are typically active at low temperatures, atypical low temperature-active enzymes are not usually denatured during production, storage, and catalytic reaction, in which thermal effects are difficult to avoid. However, atypical low temperature-active properties and related engineering of enzymes are seldom reported because of the activity–stability trade-off of enzymes [34]. This study suggests that atypical low temperature-active properties may partially ascribe to the Ω-loop rigidified by the insertion of charged amino acid residues to form salt bridges and cation–π interactions in the catalytic pocket.

Fig. 5. TLC analysis. Lanes: G, 1.0% (w/v) glucose; F, 1.0% (w/v) fructose; S and CK, inulin with the active and inactivated enzymes, respectively.

5. Conclusions

The region pertaining to the Ω-loop 5 of GH 32 was not conserved as shown by the multiple amino acid sequence alignment of seed sequences of GH 32. The exo-inulinase InuAGN25 showed a much higher frequency of charged amino acid residues in this region than that in other GH 32 members, and InuAGN25 had five consecutive charged amino acid residues (^{137}EEDRK^{141}) distinctive from the other members. The five consecutive charged amino acid residues were deleted to generate the mutant enzyme that was expressed in *E. coli*, digested by the human rhinovirus 3C protease, and purified by immobilized metal affinity chromatography. The mutagenesis broke two salt bridges, one cation-π interaction, and the α-helix–loop–310-helix structure at the N-terminal tail. The mutant enzyme showed a higher activity at low temperatures and poorer thermostability compared to that of the wild-type enzyme. These results indicate that the structural changes agree with the thermal property changes of the exo-inulinase. The study reveals the important role of the Ω-loop 5 in the thermal performance of GH 32 exo-inulinases. In the future, the five consecutive charged amino acid residues (EEDRK) may be used to insert or substitute to the Ω-loops of other GH 32 exo-inulinases for the improvement of thermostability.

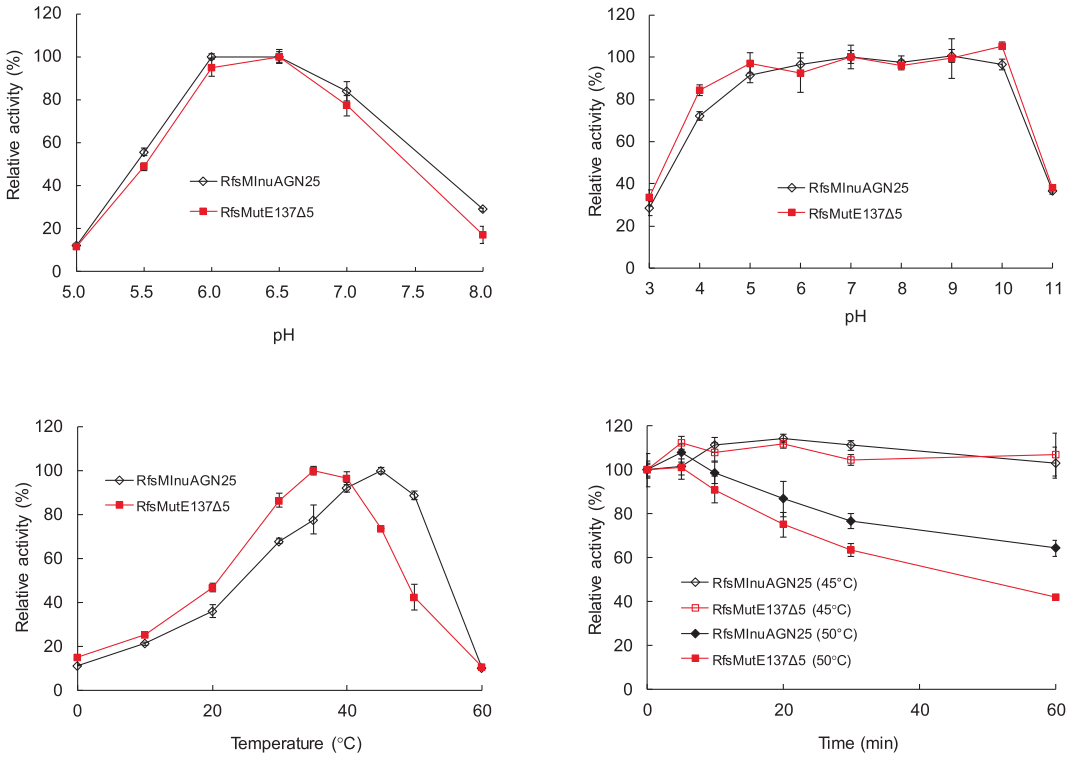

Fig. 6. Effects of pH and temperatures on the activity (a and c) and stability (b and d) of the wild-type RfsMInuAGN25 and mutant RfsMutE137Δ5. Error bars represent means ± SD (n = 3). Enzymatic properties of the wild-type RfsMInuAGN25 were characterized previously [11].

Financial support

This work was supported by the National Natural Science Foundation of China [grant numbers 31660445, 31960459], the Yunnan Fundamental Research Projects [grant number 202001AS070022], the Yunnan Ten Thousand Talents Plan Young & Elite Talents Project [grant number YNWR-QNBJ-2018-383], and the National Innovation and Entrepreneurship Training Program for College Students of China [grant number 201910681010].

Conflict of interest

The authors declare no competing financial interest.

References

[1] Singh RS, Singh T, Larroche C. Biotechnological applications of inulin-rich feedstocks. Bioresour Technol 2019;273:641–53. https://doi.org/10.1016/j.biortech.2018.11.031. PMid: 30503580.
[2] Qiu YB, Lei P, Zhang YT, et al. Recent advances in bio-based multi-products of agricultural Jerusalem artichoke resources. Biotechnol Biofuels 2018;11. https://doi.org/10.1186/s13068-018-1152-6. PMid: 29881456.
[3] Santiago M, Ramírez-Sarmiento CA, Zamora RA, et al. Discovery, molecular mechanisms, and industrial applications of cold-active enzymes. Front Microbiol 2016;7:1408. https://doi.org/10.3389/fmicb.2016.01408.
[4] Siddiqui KS. Some like it hot, some like it cold: Temperature dependent biotechnological applications and improvements in extremophilic enzymes. Biotechnol Adv 2015;33:1912–22. https://doi.org/10.1016/j.biotechadv.2015.11.001. PMid: 26585268.
[5] Zhou SH, Liu Y, Zhao YJ, et al. Enhanced exo-inulinase activity and stability by fusion of an inulin-binding module. Appl Microbiol Biotechnol 2016;100:8063–74. https://doi.org/10.1007/s00253-016-7587-4. PMid: 27164865.
[6] Nagem RAP, Rojas AL, Golubev AM, et al. Crystal structure of exo-inulinase from *Aspergillus awamori*: The enzyme fold and structural determinants of substrate recognition. J Mol Biol 2004;344:471–80. https://doi.org/10.1016/j.jmb.2004.09.024. PMid:15522299.
[7] Ma J, Li Q, Tan H, et al. Unique N-glycosylation of a recombinant exo-inulinase from *Kluyveromyces cicerisporus* and its effect on enzymatic activity and thermostability. J Biol Eng 2019;13. https://doi.org/10.1186/s13036-019-0215-y. PMid: 31737090.
[8] Zhang R, He L, Shen J, et al. Improving low-temperature activity and thermostability of exo-inulinase InuAGN25 on the basis of increasing rigidity of the terminus and flexibility of the catalytic domain. Bioengineered 2020;11:1233–44. https://doi.org/10.1080/21655979.2020.1837476. PMid: 33131413.
[9] Arjomand MR, Habibi-Rezaei M, Ahmadian G, et al. Deletion of loop fragment adjacent to active site diminishes the stability and activity of exo-inulinase. Int J Biol Macromol 2016;92:1234–41. https://doi.org/10.1016/j.ijbiomac.2016.08.039. PMid: 27527695.
[10] Zhou J, Gao Y, Zhang R, et al. A novel low-temperature-active exo-inulinase identified based on Molecular-Activity strategy from *Sphingobacterium* sp. GN25 isolated from feces of *Grus nigricollis*. Process Biochem 2014;49:1656–63. https://doi.org/10.1016/j.procbio.2014.06.013.
[11] He L, Zhang R, Shen J, et al. Removal of N-terminal tail changes the thermostability of the low-temperature-active exo-inulinase InuAGN25. Bioengineered 2020;11:921–31. https://doi.org/10.1080/21655979.2020.1809921. PMid: 32865156.
[12] Chenna R, Sugawara H, Koike T, et al. Multiple sequence alignment with the Clustal series of programs. Nucleic Acids Res 2003;31:3497–500. https://doi.org/10.1093/nar/gkg500. PMid: 12824352.
[13] Humphrey W, Dalke A, Schulten K. VMD: Visual molecular dynamics. J Mol Graph 1996;14:33–8. https://doi.org/10.1016/0263-7855(96)00018-5.
[14] Gallivan JP, Dougherty DA. Cation-π interactions in structural biology. Proc Natl Acad Sci U S A 1999;96:9459–64. https://doi.org/10.1073/pnas.96.17.9459. PMid: 10449714.
[15] Tina KG, Bhadra R, Srinivasan N. PIC: Protein interactions calculator. Nucleic Acids Res 2007;35:W473–6. https://doi.org/10.1093/nar/gkm423. PMid: 17584791.
[16] Olsson MHM, Søndergaard CR, Rostkowski M, et al. PROPKA3: Consistent treatment of internal and surface residues in empirical pKa predictions. J Chem Theor Comput 2011;7:525–37. https://doi.org/10.1021/ct100578z. PMid: 26596171.
[17] Zhao LM, Geng J, Guo YQ, et al. Expression of the *Thermobifida fusca* xylanase Xyn11A in *Pichia pastoris* and its characterization. BMC Biotechnol 2015;15:18. https://doi.org/10.1186/s12896-015-0135-y. PMid: 25887328.
[18] Xu T, Huang X, Li Z, et al. Enhanced purification efficiency and thermal tolerance of *Thermoanaerobacterium aotearoense* β-xylosidase through aggregation triggered by short peptides. J Agric Food Chem 2018;66:4182–8. https://doi.org/10.1021/acs.jafc.8b00551. PMid: 29633613.
[19] Xu H, Wang Q, Zhang ZW, et al. A simplified method to remove fusion tags from a xylanase of *Bacillus* sp. HBP8 with HRV 3C protease. Enzyme Microb Technol 2019;123:15–20. https://doi.org/10.1016/j.enzmictec.2019.01.004. PMid: 30686346.

[20] Vieille C, Zeikus GJ. Hyperthermophilic enzymes: Sources, uses, and molecular mechanisms for thermostability. Microbiol Mol Biol Rev 2001;65:1–43. https://doi.org/10.1128/MMBR.65.1.1-43.2001. PMid: 11238984.
[21] Yu HR, Huang H. Engineering proteins for thermostability through rigidifying flexible sites. Biotechnol Adv 2014;32:308–15. https://doi.org/10.1016/j.biotechadv.2013.10.012. PMid: 24211474.
[22] Zhou HY, Yong J, Gao H, et al. Loops adjacent to catalytic region and molecular stability of Man1312. Appl Biochem Biotechnol 2016;180(1):122–35. https://doi.org/10.1007/s12010-016-2087-7. PMid: 27193255.
[23] Pucci F, Rooman M. Physical and molecular bases of protein thermal stability and cold adaptation. Curr Opin Struct Biol 2017;42:117–28. https://doi.org/10.1016/j.sbi.2016.12.007. PMid: 28040640.
[24] Gavrilov Y, Dagan S, Levy Y. Shortening a loop can increase protein native state entropy. Proteins 2015;83:2137–46. https://doi.org/10.1002/prot.24926. PMid: 26369935.
[25] Damnjanović J, Nakano H, Iwasaki Y. Deletion of a dynamic surface loop improves stability and changes kinetic behavior of phosphatidylinositol-synthesizing Streptomyces phospholipase D. Biotechnol Bioeng 2014;111:674–82. https://doi.org/10.1002/bit.25149. PMid: 24222582.
[26] Dagan S, Hagai T, Gavrilov Y, et al. Stabilization of a protein conferred by an increase in folded state entropy. Proc Natl Acad Sci USA 2013;110:10628–33. https://doi.org/10.1073/pnas.1302284110. PMid: 23754389.
[27] Siddiqui KS. Defying the activity-stability trade-off in enzymes: Taking advantage of entropy to enhance activity and thermostability. Crit Rev Biotechnol 2017;37:309–22. https://doi.org/10.3109/07388551.2016.1144045. PMid: 26940154.
[28] Liu WN, Tu T, Gu Y, et al. Insight into the thermophilic mechanism of a glycoside hydrolase family 5 β-mannanase. J Agric Food Chem 2019;67:473–83. https://doi.org/10.1021/acs.jafc.8b04860. PMid: 30518205.
[29] Tu T, Li YQ, Su XY, et al. Probing the role of cation-π interaction in the thermotolerance and catalytic performance of endo-polygalacturonases. Sci Rep-UK 2016;6:38413. https://doi.org/10.1038/srep38413. PMid: 27929074.
[30] Singh RS, Chauhan K, Kennedy JF. A panorama of bacterial inulinases: Production, purification, characterization and industrial applications. Int J Biol Macromol 2017;96:312–22. https://doi.org/10.1016/j.ijbiomac.2016.12.004. PMid: 27932256.
[31] Kango N, Jain SC. Production and properties of microbial inulinases: Recent advances. Food Biotechnol 2011;25:165–212. https://doi.org/10.1080/08905436.2011.590763.
[32] Zhou J, Lu Q, Peng M, et al. Cold-active and NaCl-tolerant exo-inulinase from a cold-adapted *Arthrobacter* sp. MN8 and its potential for use in the production of fructose at low temperatures. J Biosci Bioeng 2015;119:267–74. https://doi.org/10.1016/j.jbiosc.2014.08.003. PMid: 25266375.
[33] Feller G, Gerday C. Psychrophilic enzymes: Hot topics in cold adaptation. Nat Rev Microbiol 2003;1:200–8. https://doi.org/10.1038/nrmicro773. PMid: 15035024.
[34] Yu H, Dalby PA. Exploiting correlated molecular-dynamics networks to counteract enzyme activity-stability trade-off. Proc Natl Acad Sci USA 2018;115:E12192–200. https://doi.org/10.1073/pnas.1812204115. PMid: 30530661.